Publication P3

Ville Renvall. 2009. Functional magnetic resonance imaging reference phantom. Magnetic Resonance Imaging, volume 27, number 5, pages 701-708.

Available online at www.sciencedirect.com
ScienceDirect
Magnetic Resonance Imaging 27 (2009) 701 – 708
MAGNETIC RESONANCE IMAGING

Functional magnetic resonance imaging reference phantom☆

Ville Renvall*

Advanced Magnetic Imaging Centre, Helsinki University of Technology (TKK), P.O. Box 3000, FI-02015 TKK, Espoo, Finland
Brain Research Unit, Low Temperature Laboratory, Helsinki University of Technology (TKK), P.O. Box 3000, FI-02015 TKK, Espoo, Finland

Received 14 May 2008; revised 10 September 2008; accepted 10 November 2008

Abstract

Functional magnetic resonance imaging (fMRI) is widely used to pinpoint active brain areas. Changes in neuronal activity modulate the local blood oxygenation level, and the associated modulation of the magnetic field homogeneity can be detected with magnetic resonance imaging. Thus, the blood oxygenation level-dependent (BOLD) fMRI indirectly measures neuronal activity. Similar modulation of magnetic field homogeneity was here elicited by other means to generate a BOLD-like change in a new phantom constructed to provide reference activations during fMRI. Magnetic inhomogeneities were produced by applying current to coils located near the phantom containing 1.5 ml of Gd-doped water. The signal-to-noise ratio of the images, produced by gradient-recalled echo-planar imaging, varied between 104 and 107 at a selected voxel when the field was and was not inhomogenized, respectively. The contrast of signals between homogeneous and inhomogeneous conditions was generally stable, except in 3% of time points. During the periods of greatest deviations an observable change would have been detected in a simultaneously measured BOLD signal. Such changes could result from the imaging method or occur through glitches in hardware or alterations in the measurement environment. With identical measurement setups, the phantom could allow comparing intersession or intersubject brain activations.

Keywords: Quality assurance; AMI phantom; Reference signal; BOLD phantom; fMRI; Magnetic field inhomogeneity

1. Introduction

Functional magnetic resonance imaging (fMRI) is an increasingly used brain-imaging tool. Neuronal activity modulates the supply of oxygenated blood to the active brain region, and the associated changes in magnetic field homogeneity can be detected with blood oxygenation level-dependent (BOLD) fMRI. Thus BOLD fMRI can indirectly measure variations in neuronal activity [1].

Because several factors besides neuronal activity can affect the fMRI signal, it would be important to improve the division of signal change to actual BOLD and external factors. The signal-to-noise ratio, which depends on the quality of the signal and of the measurement environment, can be improved by signal processing, e.g., by removing drifts and other implausible signal components by filtering. However, at the same time some interesting physiological signals may be removed as well. Additional monitoring methods and devices are thus needed to explain the remaining uncertainty of the measurements.

One possibility is to use an independent reference signal from, e.g., an fMRI phantom that physically imitates the fMRI signal. An fMRI phantom can reproduce the change in overall signal level during scanning, as well as the variation of the BOLD effect. At least four fMRI phantoms have already been described [2–5] and their principles of operation demonstrated. None of them has been used to correct the fMRI signals of simultaneously scanned human subjects. In two of the phantoms [2,3], electric current was led into wires to induce a local magnetic field inhomogeneity, which decreased the intensity of magnetic resonance (MR) signal. The physical basis of this phenomenon is the following.

☆ This research has been funded by Antti and Jenny Wihuri Foundation, Academy of Finland (National Centres of Excellence Programme 2006–2011) and the Finnish Graduate School of Neuroscience.

* Brain Research Unit at Advanced Magnetic Imaging Centre, Low Temperature Laboratory, Helsinki University of Technology, P.O. Box 3000, FI-02015 TKK, Espoo, Finland. Tel.: +358 9 451 6166; fax: +358 9 451 6172.
E-mail address: ville@neuro.hut.fi.

0730-725X/$ – see front matter © 2009 Elsevier Inc. All rights reserved.
doi:10.1016/j.mri.2008.11.007

Gradient-recalled (GRE) echo-planar imaging (EPI), widely employed in fMRI, yields images weighted by T_2*, the effective transverse relaxation time. T_2* is a combination of T_2 and an inhomogeneity term T′: $1/T_2^* = 1/T_2 + 1/T' \approx 1/T_2 + \gamma \Delta B_0$, where γ is the gyromagnatic ratio of proton in conventional fMRI and ΔB_0 is the inhomogeneity of magnetic field [6].

In BOLD fMRI, the different magnetic susceptibilities of blood carrying oxy- and deoxyhemoglobin modulate T′. However, any factor affecting ΔB_0, but leaving other things equal, can modulate the signal strength in a similar manner than the BOLD effect. In two of the existing phantoms [2,3], the conductors were immersed in the MR signal source, and thus partial volume effects may have masked the T′ effect. When the inhomogenizing field acts on protons near the conductors, their gradient-encoded signal can be misplaced into the space occupied by the conductors, which is not a source of MR signal. Adding a small amount of signal to originally empty, or partially filled volume, causes considerable local contrast. Therefore, inducing the ΔB_0 from outside the MR signal source would improve the design.

The aim of the present study was to develop a phantom that would provide a useful reference signal during fMRI and could also function as a research tool. Safety, accuracy and compact size — to avoid coil loading and be useful in tight fitting coils — were identified as necessary qualities. Another requirement was that the phantom must leave brain images unaffected.

2. Methods

A new fMRI reference phantom, applied magnetic inhomogeneity (AMI) phantom, was developed. The capability to produce sufficient level of MR signal and adjusting it over time were the critical factors.

2.1. Magnetic resonance signal source

In GRE-EPI-based fMRI, the signals from small liquid volumes are often weak because susceptibility differences, $\Delta\chi$, between the surroundings and the liquid deteriorate the phase coherence of spins. When a dimension of a phantom is comparable to the corresponding voxel dimension, the boundary between the container and enclosed liquid has an impact on every voxel of the phantom. Thus, it is important to minimize the $\Delta\chi$ near the liquid by using compatible materials.

Even with carefully selected materials, images of small and complex objects acquired with EPI tend to be distorted, because air is inevitably near and material boundaries are irregular. Thus, the image of a compact phantom, consisting of liquid in a container, wires and their support structures, is prone to be affected by susceptibility-related distortion. This distortion can be reduced by adding solutes to the liquid. A small amount of some paramagnetic Gd-based contrast agent is enough to adjust the susceptibility of the liquid considerably and maximize the signal from the phantom as distortion is minimized. This section details the susceptibility optimization of the new phantom.

Several tests led to the phantom design shown in Fig. 1. The phantom includes the liquid MR signal source, enclosed by a container machined of polycarbonate. Polyurethane foam was selected as the support material, because it is mostly air yet rigid, and thus the container was surrounded by air almost equally from every direction; the total copper volume, located ≥1 mm away from the liquid, was small enough to cause inconsequential distortion despite its

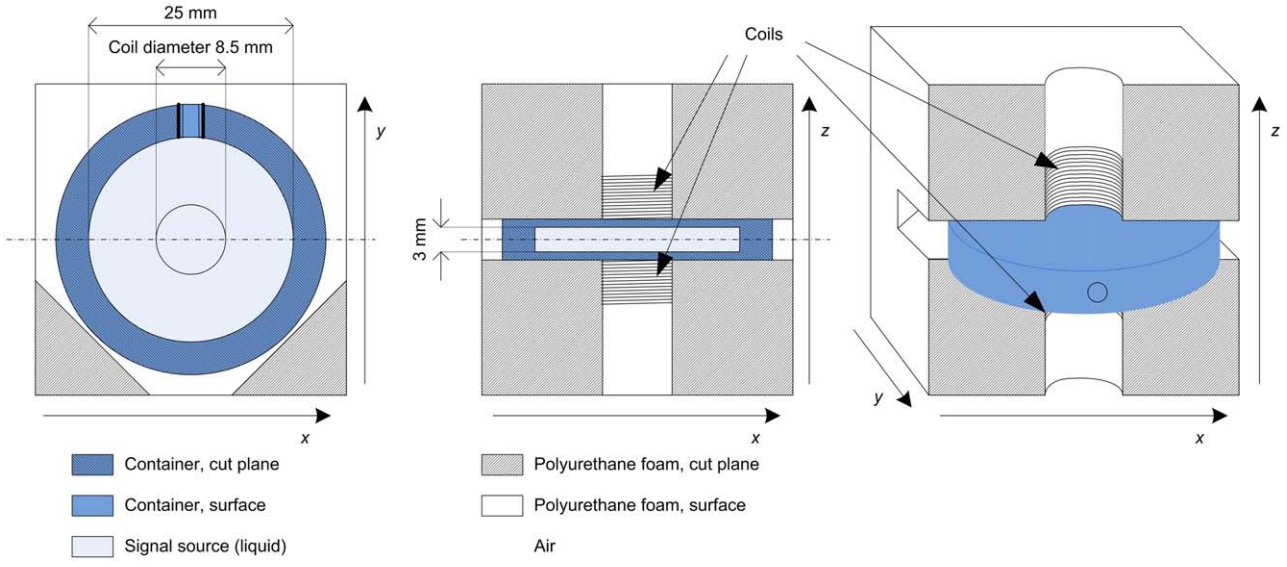

Fig. 1. The phantom consists of a block of polyurethane foam having a circular perforation onto which the cylindrical coils are attached. It also includes the plastic container and the enclosed signal source. In the rightmost picture the polyurethane block and the coils are cut at the middle; the illustration is not exact.

deviant susceptibility. Still, because of small impurities, defects in machining and the geometry dependence of the effects of different susceptibilities, the composition of the liquid had to be optimized with experimental approach.

In dilute solutions, combined susceptibility of several solution components obeys Wiedemann's additivity law:

$$\chi_m = \sum_i \chi_{m,i} p_i , \quad (1)$$

where $\chi_{m,i}$ and p_i are the mass susceptibilities and weight fractions of solution components [7,8]. Here the two-component liquid consisted of ion-exchanged water (Akkuvesi, Berner Oy Automotive, Helsinki, Finland; manufacturer-specified maximum conductance of 10 S cm^{-1}) and gadoteric acid (Dotarem, Guerbet, Villepinte, France). Dotarem contains 279.32 g L^{-1} of gadoteric acid (molecular weight 557 g mol^{-1}), whose magnetic molar susceptibility, χ_{mol}, is 2.7×10^{-2} cm^3 mol^{-1} (in CGS units). The χ_m of gadoteric acid in SI units is thus $4\times\pi\times2.7\times10^{-2}$ cm^3 mol^{-1}/557 g mol^{-1}=6.1×10^{-7} m^3 kg^{-1}. As the susceptibility of water is low, $\chi_{m,water}$=-9.05×10^{-9} m^3 kg^{-1}, even a dilute solution of the contrast agent can clearly modify the total susceptibility.

The optimal gadolinium concentration was determined experimentally by varying the concentration in the container between repeated measurements. Information about the field homogeneity within the container was obtained with EPI by zeroing the phase-encoding gradient [9], whereupon the field inhomogeneity codes the phase direction. In the solution chosen for further experiments, the concentration of gadoteric acid was 8.2 mmol L^{-1} or 4.6 g L^{-1}. The rest being mostly water, by Eq. (1), the χ_m of the resulting solution was -6.2×10^{-9} m^3 kg^{-1} or more conveniently as volume susceptibility, χ_v, -6.2×10^{-6}.

2.2. Temporal contrast

To create a BOLD fMRI-like activation–deactivation pattern in the phantom, the field homogeneity was manipulated with a pair of coils in the "Maxwell pair" configuration, as follows. The two cylindrical coils (diameter=8.5 mm, 5.4 mm long each, 28 turns) carrying current I in opposite directions produce a magnetic field, whose z-component is denoted by B_{inh} after the applied inhomogeneity. Positive current in the coils, wound anticlockwise when looked at from the container, induced B_{inh} directed at the container inside the coils' diameter.

The signaling system, controlling the applied magnetic field inhomogeneity in the phantom, comprises a transmitter outside the RF-shielded room and a receiver that resides near but outside the head coil. A light-emitting diode in the transmitter illuminates one end of an optic fiber while the transmission is ON. When the receiver detects light from the optic fiber, it sets a 6-V potential difference across its output terminals. Powering the receiver through a fiber-optic link would require regulating the voltage near the imaging target, which might interfere with the imaging. Because light intensity from an optic fiber is very sensitive to fiber alignment and movement, using the light signal directly to produce the current was infeasible. Therefore, a nonmagnetic lead battery (Yuasa NP1-6, Yuasa Battery, Inc., Laureldale, PA, USA) was selected to power the receiver. Both the input and the output of the receiver are logic gated; thus possible high-amplitude disturbances reduce to the basic output voltage of 6 V or, equivalently, to current I defined by a resistor connected in series with the output. The logic gate provides stable output amplitude, and the waveform controls the time integral of the field inhomogeneity.

2.3. Simulations

Computations (all simulations and analysis using Matlab version 6.5, Mathworks, Natick, MA, USA) helped to refine the structure of the phantom; these simulations give similar results independently of the strength of the static magnetic field of the scanner. After deciding the basic setup, the other parameters (the diameter of the coils, the distance between the coils and the number of turns in the coils) were decided based on simulations to produce a suitably shaped B_{inh}. Current driven into the coils determines the magnitude of B_{inh}; its proper value depends on the imaging parameters. For example, imaging with a 250-kHz receiver bandwidth, and with an imaging matrix sized 64×64, a voxel contains a 61-Hz frequency band in the phase-encoded direction in EPI. To modulate the precession frequency of protons by this band, the magnetic field must be adjusted by 1.4 μT, which should be clearly greater than the max(B_{inh}), to keep image distortions small.

Another simulation probed the effect of small in-plane displacements of the phantom on the reduction of phase coherence due to B_{inh}. Dephasing of spins in a 3×3×3-mm^3 voxel placed in various positions on the x-axis, while setting the y- and z-coordinates in the middle of the phantom, was computed, as a function of time. The B_{inh} was numerically integrated using the Biot–Savart law in 9261 (21×21×21) regularly spaced points, representing the spin isochromats as discretized volumes of the voxel, at each displacement. Considering each isochromat as a phasor and noting that their angular velocities are offset by $\omega=\gamma B_{inh}$, their normalized vector sum gives the fraction of phase coherence in the voxel as compared with an ideal sample.

2.4. Measurements

A 3-T whole-body MRI scanner (Signa Excite 3.0 T; GE Healthcare), utilizing an eight-channel high-resolution brain array (Signa Excite) head coil, was used in all imaging experiments. Standard pulse sequences were used throughout (software rev. E2.0_M4_0502.b).

To keep susceptibility-related distortions as uniform as possible, the current embodiment of the phantom greatly benefits from aligning the cylinder in the physical z-direction of the magnet, as shown in Fig. 1 (right). The simulations

assume this orientation, and the imaging experiments were conducted accordingly.

As both the MR signal source and the image slices were 3.0 mm thick, ideally the image stack could be positioned in the *z*-direction so that the container appeared in one slice only. Due to imperfect slice selection profile and less-than-ideal container positioning, the best option was to position the stack so that image intensity bled almost symmetrically to adjacent slices.

As described above, the composition of the liquid was optimized with imaging. Single-shot slice selection and GRE EPI readout with the following imaging parameters yielded the required information: repetition time (TR) 3 s, echo time 30 ms, nominal flip angle 90°, acquisition matrix 64×64, field of view 24 cm, slice thickness 3.0 mm without gaps between the five axial slices acquired in interleaved order, with no averages. Four dummy volumes preceded the collection of the actual data. The final composition of the liquid was selected from 11 iterations, based on the general shape of the phantom in the normal image, and the spread of the signal in the image with no phase-encoding gradient.

In the series of EPI performed to investigate the image characteristics over time, the imaging parameters were the same as above with the exceptions of TR of 2 s, field of view of 20 cm, four axial interleaved slices, number of dummy volumes of 10 and omission of the imaging with no phase encoding. In this setup, a bottle containing about 8 dl of ion-exchanged water was resting in the head coil as a simulation of the primary imaging target and the fMRI phantom was attached inside the head coil on the "patient left". The AMI was time locked with the pulse sequence (utilizing Presentation, Neurobehavioral Systems, Inc., Albany, CA, USA), and the phantom was inactive (OFF) and active (ON) in 1-TR blocks, respectively. The activation–deactivation pattern was repeated 900 times. When active, a constant current of 190 μA was driven in the coils.

2.5. Analysis

In the functional imaging experiment, the image intensity, *S*, was recorded at the voxel selected as the region of interest, and the linear drift and the baseline were removed from it; *S* designates both the original and the processed image intensity. Point-by-point differences of successive measurements, ΔS, were computed along the time course. The series of ΔS's measure the temporal variation of functional sensitivity or, if measured from a brain, the variation of BOLD contrast. The 10-point moving average of ΔS was compared with the standard deviation (S.D.) of ΔS. Block-design fMRI experiments often utilize blocks of length in the order of 10 TRs; thus the comparison tells where such a block would yield less (or more) statistical power than on the average. The signal-to-noise ratios, average of *S* minus linear drift divided by average *S* of an area of background noise over the whole time course, at both OFF and ON conditions were computed.

The analyst can choose the region of interest so that the signal-to-noise ratio and ΔS of the region are of suitable magnitude in comparison with functional data from a brain. The selected region should be sufficiently far from the borders of the phantom in the image plane to avoid contrast due to misregistration. In intersession or intersubject studies, the region of interest must remain the same in all cases.

3. Results

Fig. 2 shows the imaging results of the container filled with solutions of varying contrast agent concentrations; five of the 11 cases are presented. With the chosen concentration,

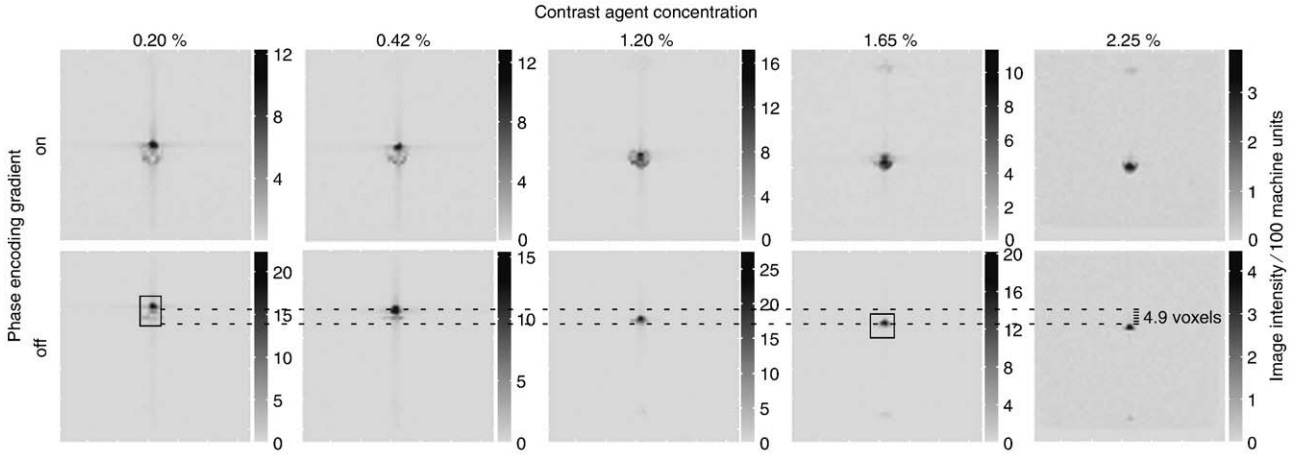

Fig. 2. Echo planar images of the phantom with different concentrations of contrast agent. The upper row shows the phase-encoded images, while in the lower row the phase (vertical) direction has been due to inhomogeneities only. Notice the different image intensity scales, thus signal-to-noise ratios, for the cases. The location of the phantom in the phase-encoded direction changes as a function of contrast agent concentration, as it should, because the resonance frequencies of the solutions differ. The dashed lines indicate the positions of the centroids of image intensities of the regions marked with black rectangles. The separation of the lines is 4.9 voxels.

1.65 vol% or 8.2 mmol L^{-1} of gadoteric acid, the overall signal level from the phantom was good and the shape of the liquid compartment remained relatively undistorted, which is evident also in the inhomogeneity image. Applying Eq. (1), the difference in χ_v between the chosen solution and the solution having 0.20 vol% of gadoteric acid predicted a 5.2 voxel shift in the phase-encoded direction with the imaging parameters used; the centroids of the image intensities calculated from the regions of interest, shown in Fig. 2, were 4.9 voxels apart. The result is in fair agreement with theory, considering the phantom had to be removed and repositioned on the support between measurements.

The Maxwell pair coil configuration can produce B_{inh} with considerable radial homogeneity near the axis of the cylinder as shown in Fig. 3, where the simulation is for the geometry of the apparatus. The wider the homogeneous area was, the further the induced fringe field extended in the computation, indicating distortion in the rest of the image. The axial change of B_{inh} ($\partial B_{inh}/\partial z$, if the phantom is aligned along the z-direction) was also quite linear, which was a desired property, because then the field distortions at material boundaries could be accounted for as easily as possible.

The placement of the imaging volume affects the phase loss induced by the phantom. For instance, as illustrated in Fig. 4, 30 ms after excitation, a 3×3×3-mm^3 voxel located exactly in the center of the phantom shows 48% of the phase coherence as compared with an identical but unaffected voxel — it takes 34 ms for the phase coherence to drop to $1/e$. A voxel affected the most is never more than 2.1 mm displaced, 1.5 mm in both x- and y-directions, where the signal intensity is at 54%.

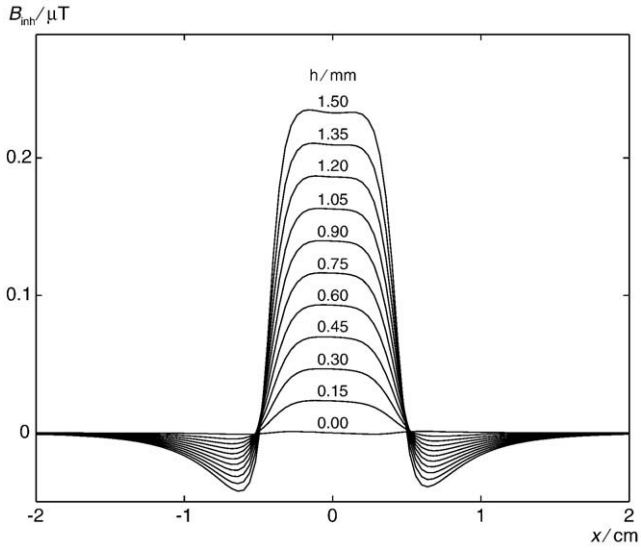

Fig. 3. The field induced by the coils as computed from the Biot–Savart law. The x-axis is the distance from the axis of the cylindrical container; B_{inh} is the z-component of the magnetic field induced with I=190 μA when the height h is the distance from the center of the container. The field beyond the values shown is not of importance because the liquid in the container does not extend beyond ±1.5 mm. Negating h negates B_{inh}.

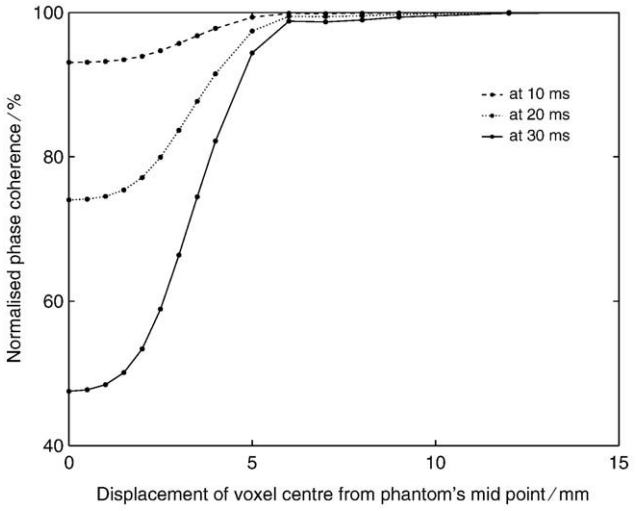

Fig. 4. Computer simulation of the phase loss introduced by the applied magnetic inhomogeneity utilized in the experiments. The computational voxel, 3×3×3 mm^3, is located at the exact middle of the container in the y- and z-directions and the displacement on the x-axis is varied.

Fig. 5 illustrates the setup of the functional imaging of the phantom, the region of interest and the area for determining the noise of the experiment. Fig. 6 shows the time course of S and ΔS of the voxel selected as the region of interest. The mean signal, corrected by removing a linear component, was 2310±5 (S±S.D.), and the signal-to-noise ratios at OFF and ON conditions were 107 and 104. The ΔS was 53±7. During

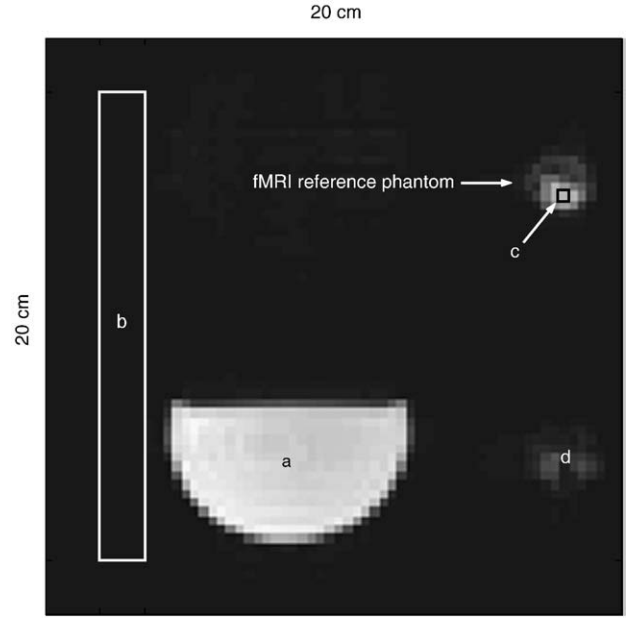

Fig. 5. A single image acquired with EPI: the small structure in the upper corner is the AMI phantom and the large structure (a) is the water bottle. The white rectangle (b) represents the voxels from which image noise was obtained; the voxel selected for computations is marked by the black outline (c). The object appearing directly below the AMI phantom (d) is the Nyquist ghost artefact of the phantom.

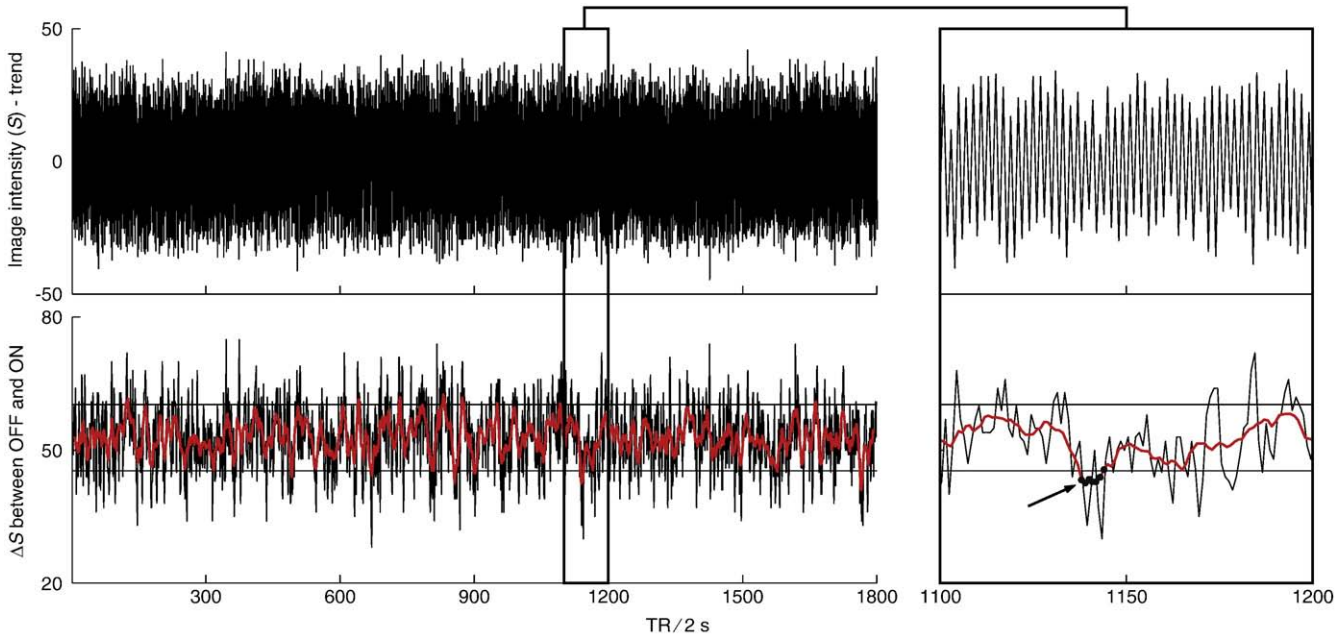

Fig. 6. The graphs on the left show the image intensity (S) and its change (ΔS) of the whole time course; on the right is shown a zoom-in of the section in black frames. The 10-point moving average of ΔS is drawn in red and the horizontal lines in the lower panels designate the ΔS±S.D. At the times of the black dots (bottom-right, an arrow pointing), the statistical power gained would be substandard.

the experiments, the variation of 10-point moving average of ΔS remained within the bounds of the standard deviation of ΔS most of the time; at 3% of time points the variation exceeded the standard deviation. Range of the 10-point moving average of ΔS was 22.

4. Discussion

A new fMRI reference phantom and a method to gain information on the functional sensitivity of the scanner were presented. Between the OFF and ON conditions, the signal from the phantom varied as expected, and the changes in the variation remained mostly within the noise level during the experiment. For monotonous repetition of standard GRE EPI sequence, low variation should be the normal finding — otherwise, the scanner or the environment would not be suitable for functional imaging. At the times when the sensitivity varied, however, such signal occurring in the brain could be regarded as physiological or would at least go unaccounted for, if it was not referenced against a phantom. As many fMRI studies are conducted with less and less averaging and complicated stimuli, the fMRI reference phantom can help to explain some expected but missed BOLD responses.

The sensitivity is prone to vary when imaging parameters are inconstant during the TRs within a time course, for example, when the scanning is halted and subsequently resumed. Also, some imaging strategies involve k-space with sparsely sampled regions, so that scanning the entirety of k-space is distributed among many TRs (e.g., Zaitsev et al. [10] describe a “keyhole” EPI technique, where every nth k-space line outside the keyhole is scanned per TR, and the whole of k-space is sequentially filled). While the overall signal-to-noise ratio may remain constant during different TRs, the sensitivity of the component images to detect functional changes may be periodically varying. Also, manually or physiologically triggered, such as cardiac gated, imaging produces time courses with varying functional sensitivity, mainly because of differences in longitudinal magnetization remaining from the previous sequence repetition, which can actually be modeled to improve the discernability of activations [11]. Whenever the imaging consists of anything else than uniform repeat of an imaging sequence, the admixture of physical parameters in the imaging equation alternates; in particular, the relative contribution of T_2* varies. With the phantom, the functional sensitivity can still be traced because the phantom physically takes into account spin history and all the complications on the imaging equation.

Studying sensitivity changes in these examples benefits from cleverer techniques than just alternating the phantom between ON and OFF conditions during successive TRs. How to use the phantom exactly, and how to analyze the phantom data, depends on the experiment, where the phantom is to be included in the prescribed imaging volume. One way to improve a cardiac-gated experiment is described in the following as an example. Let the interval between two successive TRs be τ, and the phantom be ON during the following TR. The next time the interval between two TRs is $\tau \pm \delta t$, δt chosen appropriately, the phantom would be programmatically set to the OFF condition. During the

course of the experiment, a relationship between the interval and functional sensitivity would arise; to serve the purpose of an example, it is assumed here that only the TR immediately before the examined TR bears any significance to the contrast variation, but more complex dependencies between sequence repetitions can be accommodated as well.

The following describes the sources of error associated with the fMRI reference phantom: in addition to phase loss, signal modulation in a region of interest, affected by the applied magnetic inhomogeneity, has a component of signal misregistration between the region of interest and the neighboring voxels. The gain and loss of signal in this way are often symmetric and should remain stable during an experiment. Because of the thinness of the phantom, materials surrounding the MR signal source are consequential to the field homogeneity even after susceptibility matching. The middlemost part of the liquid is in the most homogeneous field, stays in phase and thus produces the most signal per volume. The signal from a voxel only partly filled with the MR signal source may increase, because miniscule amount of signal gain by mislocation increases the image intensity substantially. Moreover, local shimming effects are likely to increase or decrease the signal near material boundaries; thus the applied inhomogeneity may accidentally even correct the local field disturbances.

From the 3-mm-thick liquid compartment, very accurate information on orientation, signal mislocation and generally data relevant for the development of the phantom can be obtained. A thicker compartment would, however, make positioning and imaging of the phantom together with fMRI subjects easier as well as susceptibility differences at material interfaces less consequential. The design of the phantom can be extended to greater separation between the inhomogenizing coils without difficulties, and without making it unsuitable for tight-fitting receiver coils. As the coils, producing the temporal contrast in the phantom, are physically separate from the liquid capsule, the capsule and the filling medium can be interchanged with those best suiting the particular application.

Using the phantom in a phased array receive coil, as was used here, produces information mainly from the nearby coil elements. Thus, if the source of signal variation is in the detection hardware, several specimens must be placed in the scanner. In that case, their thicknesses should be greater than 3 mm to make image prescription feasible, because even with a perfect phantom support stand, realistic gradient nonlinearities would make thinner phantoms appear unequally in the image plane.

It remains to be seen whether the measured sensitivity pattern can be directly applied to correcting data when the phantom has been measured concurrently with a human under fMRI. At the very least, the phantom can provide valuable criteria to keep or discard (parts of) a measurement, if for instance the sensitivity changed a lot, or to validate the filtering of certain frequency bands out of the data.

To compare intersubject or intersession variability of BOLD responses, the phantom must be mounted carefully to the imaging hardware so that it is identically positioned between sessions. These kinds of comparisons benefit from identical imaging settings including the positioning of the imaging stack, which is an uncustomary procedure, but often acceptable in fMRI, where the dicing of the volume is less critical than in diagnostic structural imaging. Comparisons between pulse sequences and imaging parameters, scanners and coils as well as the aforementioned measurement of intrameasurement variability are thought to be fruitful applications as well. The information from the phantom should enable separation of psychological, pharmacological or physiological effects, such as changes in alertness due to sedation or tiring, from external factors affecting the sensitivity of the scanner.

5. Conclusions

The fMRI reference phantom presented included a compact compartment for the liquid acting as the MR signal source; the thickness of the phantom was selected to correspond to a typical slice thickness so that identification and correcting through-plane distortion would be trivial, although a thicker phantom was envisioned to be useful in practical applications. A magnetic field inhomogeneity, from outside the container, modulated the signal emanating from the phantom. By periodical modulation of ΔB_0 in the phantom, placed in the field of view during fMRI, the MR signal from the phantom may expose unphysiological temporal signal variation and differences in activations between measurements. Ideally, two different modulation levels would be detected as two fixed signal levels. Measuring the deviation from this ideal using the AMI phantom could reveal otherwise undetectable variation in scanner's sensitivity to local signal changes. In addition, excessive filtering potentially applied to an fMRI time series may be noticed from the identically filtered reference signal.

Acknowledgments

I thank Prof. Riitta Hari for discussions and comments on the manuscript; Prof. Raimo Sepponen and Docent Gösta Ehnholm for expert advice during the research; Dr. Catherine Nangini for comments on the language; and Drs. Antti Tarkiainen, Veikko Jousmäki and Raimo Joensuu, Ms. Jaana Hiltunen and Ms. Marita Kattelus for discussions. Mr. Markku Korhonen and Mr. Juhani Kaasinen from the workshop of Low Temperature Laboratory at TKK machined several iterations of the container.

References

[1] Ogawa S, Lee TM, Kay AR, Tank DW. Brain magnetic resonance imaging with contrast dependent on blood oxygenation. Proc Natl Acad Sci U S A 1990;87:9868–72.

[2] Koopmans P, Lanting C, Versluis M, Hoogduin H. Development of a reference phantom for fMRI studies. Proceedings of the 12th Annual Meeting of ISMRM, Kyoto, Japan; 2004. p. 1039.
[3] Renvall V, Joensuu R, Hari R. Functional phantom for fMRI: a feasibility study. Magn Reson Imaging 2006;24:315–20.
[4] Cheng H, Zhao Q, Duensing GR, Edelstein WA, Spencer D, Browne N, et al. SmartPhantom—an fMRI simulator. Magn Reson Imaging 2006; 24:301–13.
[5] Olsrud J, Nilsson A, Mannfolk P, Waites A, Ståhlberg F. A two-compartment gel phantom for optimization and quality assurance in clinical BOLD fMRI. Magn Reson Imaging 2008;26:279–86.
[6] Wielopolski PA, Schmitt F, Stehling MK. Echo-planar imaging pulse sequences. In: Schmitt F, Stehling MK, Turner R, editors. Echo-Planar Imaging. Berlin Heidelberg: Springer-Verlag; 1998. p. 65–139.
[7] Mulay LN. Magnetic Susceptibility. New York: Interscience Publishers; 1963.
[8] Bakker CJG, de Roos R. Concerning the preparation and use of substances with a magnetic susceptibility equal to the magnetic susceptibility of air. Magn Reson Med 2006;56:1107–13.
[9] Mattila S, Renvall V, Hiltunen J, Kirven D, Sepponen R, Hari R, et al. Phantom-based evaluation of geometric distortions in functional magnetic resonance and diffusion tensor imaging. Magn Reson Med 2007;57:754–63.
[10] Zaitsev M, Zilles K, Shah NJ. Shared *k*-space echo planar imaging with keyhole. Magn Reson Med 2001;45:109–17.
[11] Guimaraes AR, Melcher JR, Talavage TM, Baker JR, Ledden P, Rosen BR, et al. Imaging subcortical auditory activity in humans. Hum Brain Mapp 1998;6:33–41.